Dynamical aspects of multi-round horseshoe-shaped homoclinic orbits in the RTBP

E. Barrabés*, J.M. Mondelo†, M. Ollé‡

December 9, 2008

Abstract

We consider the planar Restricted Three-Body problem and the collinear equilibrium point L_3, as an example of a center×saddle equilibrium point in a Hamiltonian with two degrees of freedom. We explore the existence of symmetric and non-symmetric homoclinic orbits to L_3, when varying the mass parameter μ. Concerning the symmetric homoclinic orbits (SHO), we study the multi-round, m-round, SHO for $m \geq 2$. More precisely, given a transversal value of μ for which there is a 1-round SHO, say μ_1, we show that for any $m \geq 2$, there are countable sets of values of μ, tending to μ_1, corresponding to m-round SHO. Some comments on related analytical results are also made.

Keywords: invariant manifolds, multi-round homoclinic orbits, Restricted Three–Body Problem.

1 Introduction

It is well known that homoclinic and heteroclinic connections of hyperbolic objects play an important role in the study of dynamical systems from a global point of view. They are also relevant in applications to celestial mechanics and astrodynamics, specially in the design of libration point mission (see e.g. Howell et al. (1998); Gómez et al. (2004); Parker and Lo (2006); Gómez et al. (2003) and references therein).

In this paper we will consider the circular Restricted Three–Body Problem (RTBP). We will restrict our attention to the collinear libration points. Since the linear character of the flow around them is center×center×saddle, the collinear points have a 4–dimensional center manifold, which, in particular, hosts all the nominal trajectories interesting for libration point missions. Periodic orbits and tori contained in the center manifold inherit the hyperbolic behavior of the equilibrium point. Thus they have stable and unstable manifolds, and their intersections give rise to homoclinic and heteroclinic orbits.

In part due to their interest for astrodynamical applications, most attention for homoclinic and heteroclinic phenomena related to libration points of the RTBP has been

*Dept. Informàtica i Matemàtica Aplicada. Universitat de Girona, Avda. Lluís Santaló s/n, 17071 Girona, Spain. barrabes@ima.udg.edu

†IEEC & Dept. Matemàtiques. Universitat Autònoma de Barcelona, Edifici C, 08193 Bellaterra, Spain. jmm@mat.uab.es

‡Dept. de Matemàtica Aplicada I. Universitat Politècnica de Catalunya, Diagonal 647, 08028 Barcelona, Spain. merce.olle@upc.edu

focused to L_1 and L_2. From the theoretical point of view, many works prove the existence of homoclinic and heteroclinic phenomena in particular situations (see e.g. Bernard et al. (2003); Mcgehee (1969); Llibre et al. (1985), and Wilczak and Zgliczyński (2003, 2005) for computer–assisted proofs). Numerical computations of homoclinic and heteroclinic connections of periodic and quasi–periodic solutions around $L_{1,2}$ have been done in the literature by means of the use of semi-analytical techniques (Gómez and Masdemont, 2000; Canalias and Masdemont, 2006; Gómez et al., 2005; Koon et al., 2000; Gómez et al., 2004; Canalias, 2007) or by 'ad hoc' continuation methods (Barrabés et al., 2008).

The L_3 case has been much less investigated, although horseshoe motion, explaining the motion of the co-orbital satellites, Janus and Epimetheus, of Saturn (see Llibre and Ollé, 2001) and near Earth asteroids (see Connors et al., 2002), has drawn some attention. The computation of horseshoe periodic orbits (HPO) in the RTBP has been done by several authors, see for example Schanzle (1967), or Taylor (1981) where some families of horseshoe periodic orbits are shown for the Sun-Jupiter mass ratio. More recently, in Barrabés and Mikkola (2005), the computation and description of the organization of families was done, and in Barrabés and Ollé (2006), the existence of symmetrical HPO in the planar RTBP from the dynamical behavior of the invariant manifolds of L_3 was studied. Furthermore, there is numerical evidence (Farrés, 2005; Gómez et al., 2001; Simó, 2006) on the fact that the stable and unstable manifolds of the objects (Lyapunov periodic orbits and 2D tori) of the center manifold of L_3 in the 3D RTBP confine regions of effective stability around the triangular points L_4 and L_5.

In this paper, we will deal with the simplest case, that is, we consider from now on the planar RTBP. We want to analyze the existence of homoclinic orbits to the equilibrium point L_3 itself, when varying the mass parameter μ. This study has two main motivations. On the one hand, the dynamics of the stable and unstable 1–dimensional manifolds of L_3 may be regarded as the skeleton or as a clue in order to know the dynamics of the invariant manifolds of the periodic and quasi-periodic orbits close to the equilibrium point. In particular, Lerman proved, under generic conditions, the existence of homoclinic orbits to each hyperbolic Lyapunov periodic orbit in the presence of a homoclinic orbit to a saddle×center equilibrium point (in a Hamiltonian with two degrees of freedom), see Lerman (1991). This problem is revisited in Bernard et al. (2003) in the case in which there is not a homoclinic orbit to a saddle×center equilibrium point. In Koltsova et al. (2005), the authors analyzed the homoclinic orbits to invariant tori near a homoclinic orbit to a center×center×saddle equilibrium point (in a Hamiltonian with three degrees of freedom). On the other hand, the existence of an infinite set of periodic orbits accumulating to a given homoclinic orbit (the so called blue sky catastrophe phenomenon after Devaney, see Devaney (1977) and also explains the evolution of some families of horseshoe periodic orbits, when varying the mass parameter μ and the Jacobi constant C (see Barrabés and Ollé, 2006).

The paper is structured as follows. Section 2 states the conventions followed for the RTBP, the libration points and the Jacobi constant. Section 3 explores the existence of homoclinic orbits to L_3, both symmetric and non-symmetric, in the interval $[.0002, .02]$ that contains the Earth-Moon ($\mu = 0.01215$) and Sun-Jupiter ($\mu = 0.000953875$) mass parameters. The rest of the paper is devoted to a numerical study of the cascades of multi–round homoclinic connections accumulating to horseshoe–like homoclinic connections of L_3, that are predicted by the theoretical results in the references mentioned above. By analyzing orthogonal crossings to the $\{y = 0\}$ axis, we derive a graphical procedure that

allows to locate the value of μ corresponding to the homoclinic connection in any level of the cascade. In this way, one–round homoclinic connections are studied in Section 4, two–round in Section 5, and m–round, for $m \geq 2$, in Section 6.

2 The RTBP

The circular, restricted three–body problem (RTBP) describes the motion of a particle of infinitesimal mass, moving under the gravitational influence of two massive bodies called primaries, that describe circular orbits around their common center of mass. We will consider the planar problem, in which the motion of the third body is contained in the plane of motion of the primaries. Taking a coordinate system reference that rotates with the primaries, with origin placed at their center of mass, and suitable units, we can assume that the primaries have masses $1-\mu$ and μ, $\mu \in (0, 1/2]$, their positions are fixed at $(\mu, 0)$ and $(\mu - 1, 0)$ and the period of their motions is 2π. With these assumptions, the equations of motion of the third body in this rotating (also called synodical) system of coordinates, are (see Szebehely, 1967)

$$\begin{array}{rcl} x'' - 2y' & = & D_x\Omega(x,y), \\ y'' + 2x' & = & D_y\Omega(x,y), \end{array} \tag{1}$$

where

$$\Omega(x,y) = \frac{1}{2}(x^2+y^2) + \frac{1-\mu}{r_1} + \frac{\mu}{r_2} + \frac{1}{2}\mu(1-\mu),$$

$r_1 = \sqrt{(x-\mu)^2+y^2}$ and $r_2 = \sqrt{(x-\mu+1)^2+y^2}$. The system of equations (1) has a first integral, called the Jacobi integral, which is given by

$$\mathcal{C} = 2\Omega(x,y) - x'^2 - y'^2. \tag{2}$$

Furthermore, we recall that equations (1) satisfy the well known symmetry

$$(t, x, y, x', y') \quad \longrightarrow \quad (-t, x, -y, -x', y'). \tag{3}$$

This implies that, for each solution of equations (1), there also exists another one, which is seen as symmetric with respect to $y = 0$ in configuration space.

We also recall that the RTBP has five equilibrium points: the collinear points, L_1, L_2 and L_3, situated on the line containing the primaries, and the equilateral ones, L_4 and L_5, both forming an equilateral triangle with the two primaries. We recall that $x_{L_2} \leq \mu - 1 \leq x_{L_1} \leq \mu \leq x_{L_3}$, that is, L_1 is between both primaries, L_2 is on the left hand side of the small one and L_3 is on the right hand side of the large one.

We focus our attention on the collinear equilibrium point L_3, whose position and Jacobi constant (C_3) values in terms of μ are given by (see Szebehely, 1967)

$$x_{L_3} = 1 + \frac{5}{12}\,\mu + O(\mu^3), \quad C_3 = 3 + 2\mu + O(\mu^2).$$

It is well known that, if we write the differential equations (1) as

$$\mathbf{x}' = \mathbf{X}(\mathbf{x})$$

then Spec $DX(L_i) = \{\pm i\omega, \pm\lambda\}$, so the equilibrium point L_i, $i = 1, 2, 3$ is a center$\times$saddle point. This saddle part is responsible for the existence of 1-dimensional invariant manifolds associated with L_3. These unstable and stable manifolds can intersect, giving rise to homoclinic connections to L_3.

3 Homoclinic connections to the equilibrium point L_3

Let us explain the notation that will be used throughout this Section. The invariant unstable (W^u) or stable (W^s) manifold associated with the equilibrium point L_3 is 1-dimensional, and we will denote by $W_+^{u/s}$ the branch that tends (backward/forward) to the equilibrium point from the upper half region $\{y > 0\}$ and $W_-^{u/s}$ the one from the lower half region $\{y < 0\}$. Observe that, due to the symmetry (3), the branches W_-^u and W_+^s, as well as W_+^u and W_-^s, are symmetric.

In order to compute numerically a branch $W_{+/-}^u$ ($W_{+/-}^s$), we have taken as an initial condition $L_3 + s \cdot v$, where s is a small quantity, v is a unit eigenvector associated with the eigenvalue $\lambda > 0$ ($\lambda < 0$ respectively) of the Jacobian matrix of the vector field at L_3. From this initial condition, we follow the invariant manifold numerically integrating the system of ODE, forward (backward) in time under the test check that along the integration the Jacobi constant value must remain constant and equal to $C = C_3$. The computations have been done using $s = 10^{-6}$ with double precision. Most figures have been checked reproducing the computations using quadruple precision.

The exploration of the existence of symmetric and non-symmetric homoclinics to L_3 is done for values of $\mu \in [0.0002, 0.02]$. Given a value of μ, the branch $W_\pm^{u/s}$ consists of a single orbit and in order to find homoclinic connections we have to deal with one branch of each invariant manifold. It becomes natural to distinguish between four different types of homoclinic orbits, depending on which branches are involved. We consider a Poincaré section Σ fixed values $j, k \in N$, and for each value of μ we follow one branch of W^u and one branch of W^s up to the j-th and k-th crossing with the section Σ, respectively. Each intersection is a point $q_j^u(\mu) = (x^u, y^u, x'^u, y'^u)$, on the unstable branch, and $q_k^s(\mu) = (x^s, y^s, x'^s, y'^s)$ on the stable one. We define a *homoclinic orbit of type* $(+j, +k)$ if following the branch W_+^u and W_+^s up to the j-th and k-th crossing with the section Σ respectively, the condition

$$q_j^u(\mu) = q_k^s(\mu) \tag{4}$$

is satisfied. Similarly we define a homoclinic orbit of type $(+j, -k)$, $(-j, +k)$, $(-j, -k)$ by considering the suitable branches in the corresponding regions (see Fig. 2 for examples). This definition depends strongly on the section Σ considered, as we will see.

Observe that the homoclinic connections of type $(+j, +k)$ or $(-j, -k)$ are non-symmetric. Furthermore, due to the symmetry (3), if there is a non symmetric homoclinic orbit of type $(-j, -k)$, the mutually symmetric orbit is also an homoclinic connection of type $(+j, +k)$. We also remark that homoclinic connections of type $(-j, +k)$ or $(+j, -k)$ are symmetric.

Given μ, in order to check the existence of a homoclinic orbit of a given type (ie j, k and signs) we follow this simple method: we take $\Sigma = \{x = c\}$, being c a constant, and we consider the corresponding points $q_j^u(\mu) = (x^u, y^u, x'^u, y'^u)$ and $q_k^s(\mu) = (x^s, y^s, x'^s, y'^s)$ and the functions:

$$d_y(\mu) = y^u - y^s, \qquad d_{x'}(\mu) = x'^u - x'^s, \qquad d_{y'}(\mu) = y'^u - y'^s$$

since $x^u = x^s$. Observe that these functions depend on j and k although we have skipped explicitly this dependence in the notation. We also remark, and this will be seen later on, that when we fix a j and a k, these functions may not be continuous due to the appearance

of loops in the manifolds. Taking into account the direction of the orbits at the intersection of the manifolds with the section and that the energy is the same for both branches, the condition (4) of homoclinic connection is satisfied if two of these functions are equal to zero.

When varying μ some observations with respect to the behavior of the invariant manifolds are needed.

- As μ increases, the separation between the branches increases and the minimum distance to the small primary decreases, see Fig. 1 where the projection in the (x, y) plane of the branches W^u_- and W^s_- until the first and second intersections (respectively) with Σ, for different values of μ, are plotted. In fact, for $\mu > 0.01173615$ the projection in the configuration space of the branch W^s_- enters the upper half region $\{x < 0, y > 0\}$. This means that for $\mu > 0.01173615$, the dynamics around the small primary and the equilibrium points L_1 and L_2 play a role (and the corresponding Lyapunov orbits and their invariant manifolds). In particular, there exist values of μ for which one of the invariant manifolds collides with the small primary (see Barrabés and Ollé, 2006) and values of μ for which there are not homoclinic but heteroclinic connections between L_3 and a Lyapunov periodic orbit around L_1 or L_2 (see Fig. 1). At these values, the functions $d_*(\mu)$ present discontinuities, so the exploration must be done carefully.

- For small values of μ, and considering few intersections with Σ, the invariant manifolds have a (half) horseshoe shape, see Fig. 1. But as μ increases, this shape is not conserved anymore and the invariant manifolds perform complete loops around the big primary, see Fig. 2. This behavior must be taken into account when considering different values for the number of intersections j and k.

- For μ small, ($\mu < 0.0002$), all functions $d_*(\mu)$ take very small values, less than 10^{-6}. For this range of values of μ, the functions $d_*(\mu)$ are very sensitive to the distance of L_3 that we have taken for the linear approximation of the invariant manifolds, due to the fact that we are dealing with a singular perturbation problem when $\mu \to 0$. We have excluded these values of our exploration.

The results obtained are summarized next, where we have typically used $\Sigma = \{x = \mu - 1/2\}$.

1. Non symmetric homoclinic orbits. As we have already said, it is enough to explore the connections of type $(-j, -k)$.

   When varying $\mu \in [0.0002, 0.01173615]$ and according to the behavior of the invariant manifolds, typically horseshoe shaped orbits, a necessary condition for the existence of homoclinic orbits is to consider $j + k \geq 3$. In particular, we study the cases $j = 1, k = 2$, $j = 2, k = 3$ and $j = 3, k = 4$. For these values, the numerical exploration does not reveal the existence of non symmetric homoclinic connections to the equilibrium point L_3. Of course, for other cases (bigger values of μ and given j, k), the same procedure might be carried out.

2. Symmetric homoclinic orbits (SHO). We now look for connections of type $(-j, +k)$ or $(+j, -k)$ (notice that a connection of type $(-j, +k)$ is also of type $(-(j-i), +(k+i))$ for any $i = 0 \dots j$, and similarly with the $(+j, -k)$ connections). We explore both couple of branches, as their shape can be very different, see Fig. 2. Again taking into

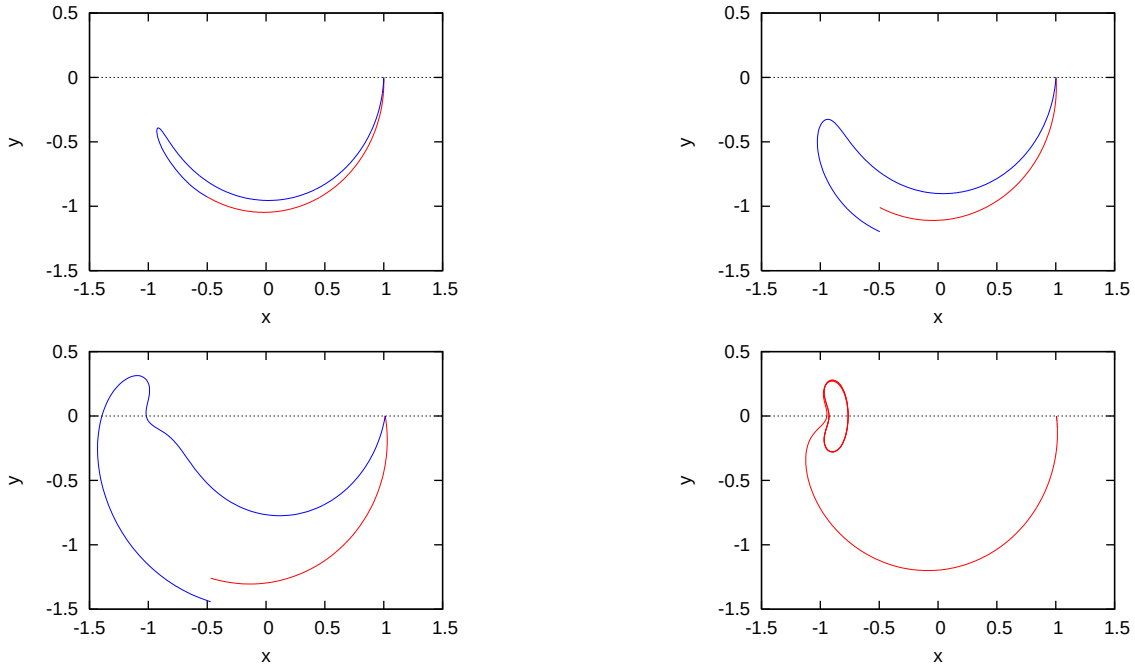

Figure 1: $\Sigma = \{x = \mu - 1/2\}$. Projection in the configuration space of the invariant manifolds of L_3 until $W^u_- \cap \Sigma^1$ and $W^s_- \cap \Sigma^2$ for $\mu = 0.001$ (top left), $\mu = 0.005$ (top right), $\mu = 0.02$ (bottom left). Bottom right: heteroclinic orbit for $\mu = 0.014562349014$. (Trajectories in W^u and W^s in red and blue respectively.)

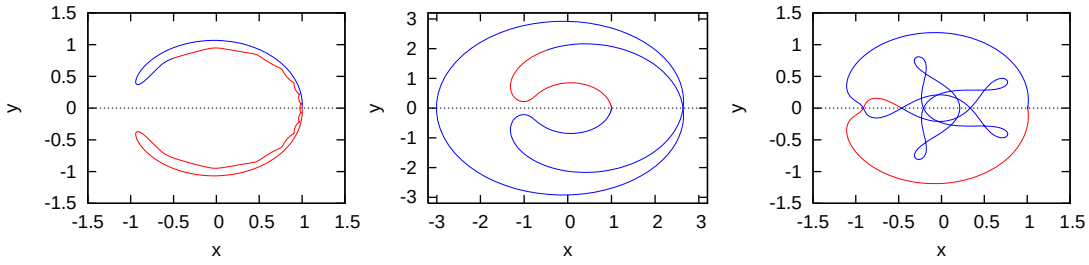

$\mu = 0.00196201$ $\quad$ $\mu = 0.012143988024852$ $\quad$ $\mu = 0.0133233$

$(-2, +3)$ $\quad$ $(+2, -5)$ $\quad$ $(-2, +3)$

Figure 2: $\Sigma = \{x = \mu - 1/2\}$. Projection in the configuration space of homoclinic connections to L_3 for the indicated values of the mass parameter and type. (Trajectories in W^u and W^s in red and blue respectively.)

account the behavior of the invariant manifolds, we look for homoclinic connections such that $j + k \geq 5$. We have explored in detail the cases $(-2, +3)$, $(+2, -5)$ and $(-4, +5)$, and we have found homoclinic connections in all of them. In Fig. 2 some of these connections are plotted. In Fig. 3 the functions $d_y(\mu)$ and $d_{y'}(\mu)$ are plotted in the cases $(-2, +3)$ and $(-4, +5)$ and for a certain range of values of μ just to show that there exist many values of the mass parameter for which an homoclinic orbit

exists. With respect to their computation it is worth doing some observations:

(a) in particular, for type $(-2,+3)$ there exists a sequence of values of μ tending to zero with an homoclinic connection to L_3. See Fig. 3 left. This will be clear in next Section.

(b) connections of type $(+2,-5)$ appear for $\mu > 0.00435846$, which is the first value of μ for which we have found a homoclinic connection of this type. This is due to the fact that these types of connections are not horseshoe shaped and this behavior appears only when μ increases. See Fig. 2 right.

(c) connections of type $(-4,+5)$ may be related to the phenomenon of double-round homoclinic orbits. See Fig. 3 right. Actually the analysis of symmetric one-round and multiple-round homoclinic orbits is the purpose of the next sections.

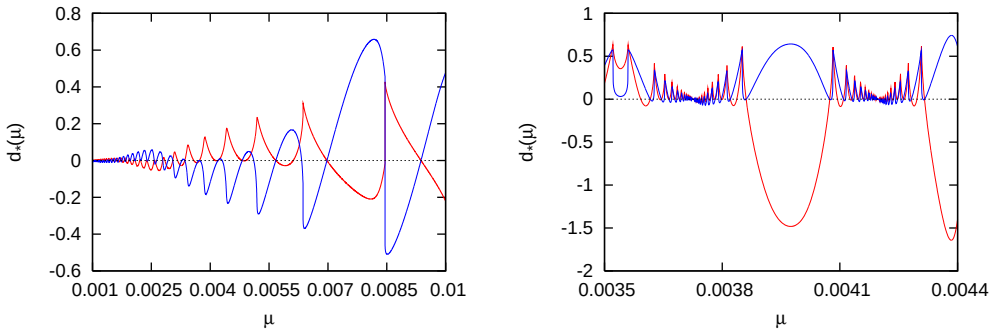

$(-2,+3)$ $(-4,+5)$

Figure 3: Functions $d_y(\mu)$ and $d_{y'}(\mu)$ for the $(\pm j, \pm k)$ cases indicated and for different range of values of μ. Each intersection of both functions at the horizontal axis for the same value of μ corresponds to a value of the mass parameter for which a homoclinic connection to L_3 exists.

4 One-round homoclinic orbits

From now on, we will consider only symmetric homoclinic orbits, SHO. For that reason, in all that follows we will consider $\Sigma = \{y = 0\}$ as surface of section. Denote by $x'_j(\mu)$ the x' coordinate of the j–th intersection of a branch of a manifold of L_3 (e.g. W^u_-) with Σ. If this j–th cut is orthogonal, that is,

$$x'_j(\mu) = 0, \tag{5}$$

the application of symmetry (3) to a trajectory following W^u_- up to its j–th cut with $y = 0$ forward in time will give rise to a symmetric trajectory following W^s_+ backward in time, which will intersect the first one at the j–th cut with the x axis, at a point with $y = x' = 0$, giving rise to a SHO.

In what follows, the $x'_j(\mu)$ functions will refer to the W^u_- branch. We will consider a one–round homoclinic trajectory as a horseshoe–shaped SHO, as in Fig. 2 left. A j–round

SHO will therefore be a homoclinic connection that surrounds j times L_3, L_4 and L_5. Define the set

$$\Lambda_j = \{\mu > 0 \,/\, \text{ there exists a j-round SHO}\}.$$

In order to detect numerically values $\mu \in \Lambda_j$ for a given j, we look for values of μ for which condition (5) is satisfied.

Let us start analyzing the set Λ_1. We vary the μ parameter and we consider the function $x_1'(\mu)$ given in Fig. 4 left. Its behavior provides numerical evidence of the existence of a decreasing sequence of values of μ, with $\mu_1^1 < 0.01$, such that $x_1'(\mu_n^1) = 0$ and $\mu_n^1 \to 0$ when $n \to \infty$, so $\mu_n^1 \in \Lambda_1$, $n \in \mathbb{N}$ (see Font (1999) for an expression of such values). For any given value of μ_n^1, the corresponding SHO (that surrounds once L_4 and L_5) has an orthogonal crossing with the {y=0} axis with $x < x_{L_3}$. From now on we call each μ_n^1 a *transversal* value since the function $x_1'(\mu)$ intersects transversally the μ axis (on the (μ, x_1') plane) at μ_n^1. In Fig. 4 right, we show a homoclinic orbit for the transversal value $\mu = \mu_n^1 = 0.0037257851523$.

We remark that the function $x_1'(\mu)$ presents jump discontinuities for some values of μ. This is due to the fact that, for μ close to each jump discontinuity, the (x, y) projection of the W_-^u branch has a loop that intersects the x axis close to L_3, see Fig. 5 (a similar figure can be found in Llibre et al. (1985)). In order to compute the values of μ for which an SHO with a loop exists, we must consider the function $x_2'(\mu)$. Consider Fig. 6, where the functions $x_1'(\mu)$ and $x_2'(\mu)$ are plotted. Inspection of the function $x_2'(\mu)$ reveals that, in a neighborhood of each discontinuity of the function $x_1'(\mu)$, a piece of the function $x_2'(\mu)$ cuts the horizontal axis. That is, there is a value of μ, that we will call *loop value* from now on, such that the corresponding unstable manifold becomes a SHO and its (x, y) projection has an orthogonal crossing just in the middle of the loop with $x < x_{L_3}$. The situation is illustrated in Fig. 5. As μ increases, the loop moves down and stops intersecting the section, so the function $x_1'(\mu)$ presents a discontinuity. However, this is a local property of the orbit, since globally the homoclinic orbit surrounds just once L_4 and L_5, so this loop value belongs to Λ_1. Fig. 5 right displays an example of such a SHO. Fig. 4 left shows the existence of a sequence of loop values of μ, that we will denote as $\mu_n^{\overline{1}} \in \Lambda_1$, such that $\mu_n^{\overline{1}} \in \Lambda_1 \to 0$ when $n \to \infty$. These values are in Λ_1 together with μ_n^1. From now on, bars will refer to loop values.

When considering the branch W_+^u, the function $x_1'(\mu)$ shows the same qualitative behavior, giving rise also to two sequences of values of $\mu \in \Lambda_1$. The actual values are different from the ones obtained with W_-^u.

In the following sections, we study the existence of multi-round homoclinic orbits. As a guide for quick references, we include here a list of notations and rules used. The sequences of values of μ for which a round homoclinic orbit exists have been labelled according the following rules:

- an overline above a number denotes that the homoclinic orbit exhibits a loop in its perpendicular intersection with the horizontal axis;
- the sign $+$ or $-$ denotes that the sequence decreases or increases, respectively.

The notations used are listed below:

- μ_n^δ, $n \in \mathbb{N}$, is a sequence, tending to zero, corresponding to a one round homoclinic orbit without/with a loop in its perpendicular intersection with the horizontal axis for $\delta = 1, \overline{1}$ respectively, as we have seen in the present Section;

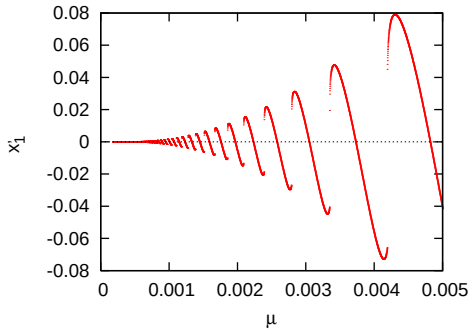

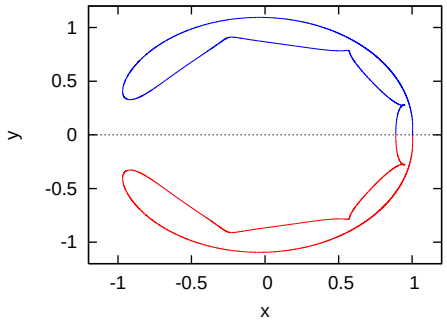

Figure 4: Left. Function $x_1'(\mu)$. Right. Homoclinic invariant manifold –(x, y) projection– for $\mu = 0.0037257851523$.

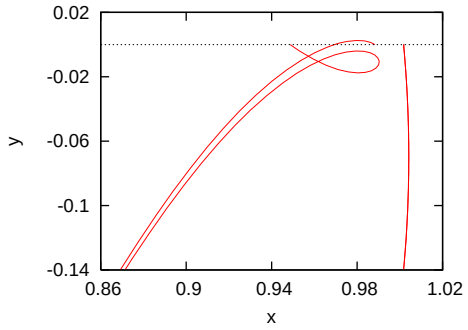

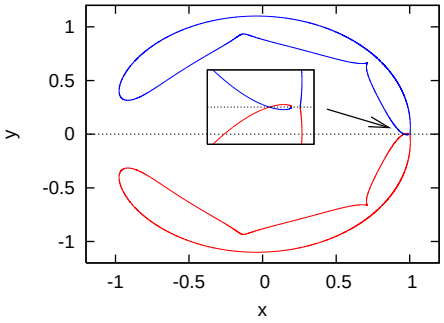

Figure 5: Left: two different unstable manifolds having a loop close to L_3 (projection in the (x, y) plane). Right: homoclinic manifold with the orthogonal crossing at half loop.

- $\mu_{n,m}^{\delta,k\pm}$, and $\mu_{n,m}^{\delta,\overline{k}\pm}$, $m \in \mathbb{N}$, are sequences, corresponding to a k-round homoclinic orbit, tending to μ_n^δ, $\delta = 1, \overline{1}$.

5 Double-round homoclinic orbits

From now on we will consider only the branch W_-^u. At the end of this Section we will comment the results obtained taking the branch W_+^u.

In order to study the existence of 2-round SHO, we start considering the function $x_2'(\mu)$. In the absence of loops, the zeros of this function will give the values of μ for which L_3 has a double–round SHO. In the presence of loops, double–round SHO will be given by the zeros of $x_j'(\mu)$ for $j \geq 3$. Fig. 6 represents the $x_1'(\mu)$ and $x_2'(\mu)$ functions simultaneously. In order to discuss it, we will distinguish between transversal and loop values in the function $x_1'(\mu)$. See also Fig. 8 for a zoom.

Close to a transversal value of μ, μ_n^1, a zoom of Fig. 6 (for example, see Fig. 8) in a neighborhood of each one of these values reveals the existence of two sequences of values of μ given by zeros of $x_2'(\mu)$. One of these sequences, that will be denoted as $\{\mu_{n,m}^{1,2-}\}_m$, is increasing, whereas the other one, that will be denoted as $\{\mu_{n,m}^{1,2+}\}_m$, is decreasing. They

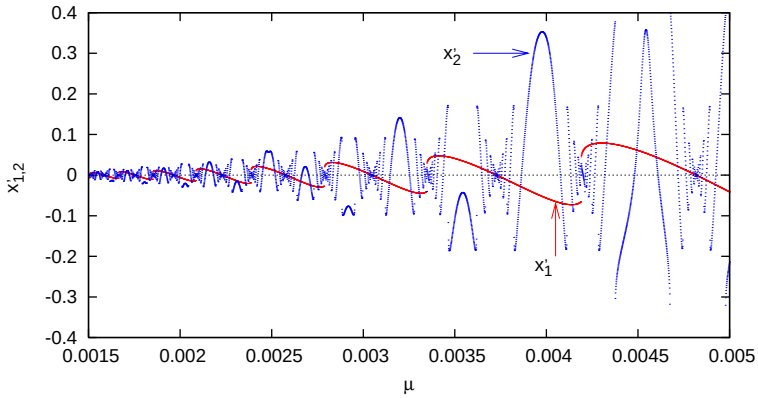

Figure 6: Functions $x_1'(\mu)$ (in red) and $x_2'(\mu)$ (blue).

satisfy

$$\mu_{n,m}^{1,2-} < \mu_n^1 < \mu_{n,m}^{1,2+}, \qquad \lim_{m\to\infty} \mu_{n,m}^{1,2-} = \lim_{m\to\infty} \mu_{n,m}^{1,2+} = \mu_n^1.$$

For each value of μ belonging to either of the sequences, the corresponding SHO (that describes two rounds) has an orthogonal crossing at the second intersection with the $\{y = 0\}$ axis with $x > x_{L_3}$. See Fig. 7 top left.

In a zoom of Fig. 6 near to a μ_n^1 value, (see Fig. 8 left) the jump discontinuities of the $x_2'(\mu)$ function that can be seen accumulating to the μ_n^1 value give two new sequences of values of μ. One of them, that will be denoted as $\{\mu_{n,m}^{1,\overline{2}-}\}_m$, is increasing, whereas the other one, which will be denoted as $\{\mu_{n,m}^{1,\overline{2}+}\}_m$, is decreasing. Together with the two previous ones, they satisfy

$$\mu_{n,m}^{1,2-} < \mu_{n,m}^{1,\overline{2}-} < \mu_n^1 < \mu_{n,m}^{1,\overline{2}+} < \mu_{n,m}^{1,2+}.$$

These two new sequences correspond to SHO that do not have a loop at the first crossing with $\{y = 0\}$, but have one at the second crossing, so that the orthogonal crossing is the third one, in a point with $x > x_{L_3}$. These SHO correspond to zeros of the $x_3'(\mu)$ function close to a jump discontinuity of the $x_2'(\mu)$ function, being in turn close to a zero of the $x_1'(\mu)$ function. An example of such an SHO is given in Fig. 7 top right.

Note in Fig. 7 top, that the two-round SHO displayed, corresponding to particular values of the sequences $\mu_{n,m}^{1,2-}$ and $\mu_{n,m}^{1,\overline{2}-}$ close to μ_n^1, closely resemble to the one associated with μ_n^1, to which both sequences tend to. We remark that the existence of such four sequences of values of μ is in accordance with the analytical results in Koltsova's paper (see Koltsova (2003)).

Consider now a loop value of μ, that is, a value in the $\mu_n^{\overline{1}}$ sequence. In this case in an interval of values of μ near $\mu_n^{\overline{1}}$ (see Fig. 8 right) for which the (x, y) projection of the W_-^u branch of the manifold of L_3 has the first three crossings with the x axis, corresponding to a loop on the left of L_3, the function $x_4'(\mu)$ has to be taken into account. This function is also represented in Fig. 8 right. In this case, by the same argument as above, we obtain again four sequences of values $\{\mu_{n,m}^{\overline{1},2\pm}\}_m$, $\{\mu_{n,m}^{\overline{1},\overline{2}\pm}\}_m$ in Λ_2, corresponding to zeros and jump discontinuities of $x_4'(\mu)$, respectively. In the case of a loop discontinuity, the exact value $\mu_{n,m}^{\overline{1},\overline{2}\pm}$ for which a SHO exists is given by a zero of $x_5'(\mu)$. See Fig. 7 bottom for a particular

two-round SHO with a loop on the left of L_3 for $\mu_{n,m}^{\overline{1},2-} = 0.004192163077$ close to $\mu_n^{\overline{1}}$.

We have also carried out the exploration of the set Λ_2 for the W_+^u branch of the manifold of L_3. We have omitted the results because the qualitative results are the same, although the values obtained for the $\{\mu_{n,m}^{1,2\pm}\}_m$, $\{\mu_{n,m}^{1,\overline{2}\pm}\}_m$, $\{\mu_{n,m}^{\overline{1},2\pm}\}_m$, $\{\mu_{n,m}^{\overline{1},\overline{2}\pm}\}_m$ sequences are different.

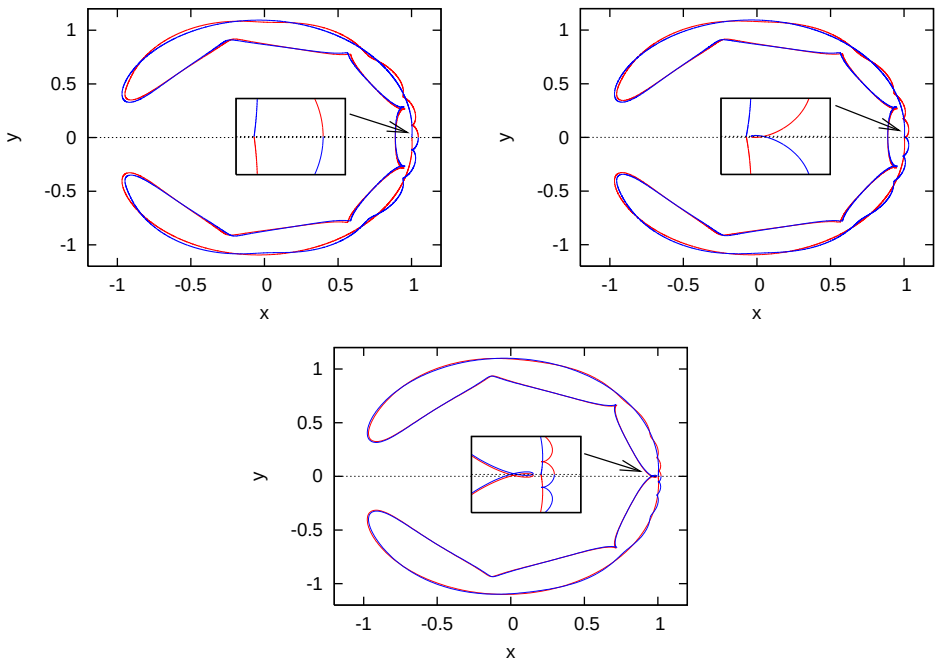

Figure 7: Top: Double-round SHO for $\mu_{n,m}^{1,2-} = 0.00371179$ (left) and for $\mu_{n,m}^{1,\overline{2}-} = 0.00371559$ (right) close to μ_n^1. Bottom: double-round SHO for $\mu_{n,m}^{\overline{1},2-} = 0.004192163077$ close to $\mu_n^{\overline{1}}$.

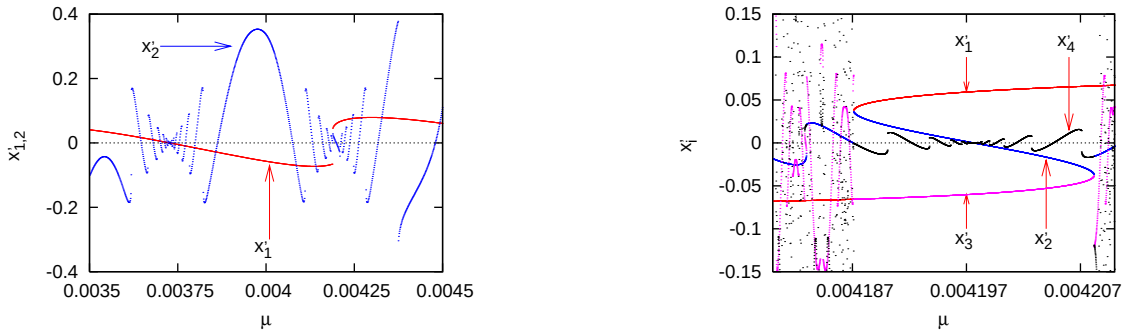

Figure 8: Left: functions $x_1'(\mu)$ and $x_2'(\mu)$ around $\mu_n^1 = 0.0037257851523$ and $\bar{\mu}_n^1 = 0.00419758$. Right: functions $x_i'(\mu)$, $i = 1, \ldots, 4$ for μ close to $\mu_n^{\overline{1}} = 0.00419758$.

6 Multi-round homoclinic orbits

From the analytical results in Grotta Ragazzo (1997); Mielke et al. (1992) a cascade phenomenon of multi-round homoclinic orbits in the parameter value μ follows, in the sense that there are not only 2–round, but also 3–round,..., k–round SHO, for any $k \in \mathbb{N}$, for values of μ tending to a value μ_n^1 or $\mu_n^{\overline{1}}$ in Λ_1. In this section we would like to illustrate this cascade phenomenon for the RTBP in terms of the $x'_j(\mu)$ functions.

Therefore we will take a particular value of μ, $\mu_l^1 = 0.0037257851523$, and we will consider a very narrow neighborhood I of it. The results for any other values μ_n^1 are qualitatively the same. See Fig. 8 left.

In order to analyze the set Λ_k, for $k \geq 3$, we compute the functions $x'_k(\mu)$, for $k = 3, 4, 5$ in I, see Fig. 9 and 10. Due to the fact that we are using the linear approximation for the manifold of L_3 and double precision, we are not able to compute numerically the function $x'_k(\mu)$ for any value of $k \in \mathbb{N}$, but the behavior of such functions when increasing k seems to follow a pattern with common properties that we now describe.

The functions $x'_k(\mu)$, for $k = 3, 4, 5$ exhibit an oscillating behavior with maximum (minimum) values of the function decreasing (increasing) to 0 as μ tends to μ_l^1. Such oscillations are the responsible for the existence of infinitely many values $\mu \in \Lambda_k \cap I$ on both sides of μ_l^1.

From the behavior of the function $x'_3(\mu)$ plotted in Fig. 9, we observe that there is one increasing sequence of values of $\mu \in \Lambda_3$ tending to μ_l^1 on the left, and another decreasing one tending to μ_l^1 on the right. These values correspond to the three zeros of the $x'_3(\mu)$ function in each interval of the form $(\mu_{l,m}^{1,\overline{2}-}, \mu_{l,m+1}^{1,\overline{2}-})$ and $(\mu_{l,m+1}^{1,\overline{2}+}, \mu_{l,m}^{1,\overline{2}+})$ that are away from the edges of the intervals (see Fig. 9 right). They give rise to two sequences $\{\mu_{l,m}^{1,3-}\}_m$ and $\{\mu_{l,m}^{1,3+}\}_m$ in Λ_3, which are increasing and decreasing, respectively. The zeros of $x'_3(\mu)$ near the edges of these intervals are exactly the values $\mu_{l,m}^{1,\overline{2}\pm}$, $\mu_{l,m+1}^{1,\overline{2}\pm}$ (see the previous Section). Very close to these zeros of $x'_3(\mu)$, there are jump discontinuities of $x'_3(\mu)$ that correspond to points in Λ_3 with a loop in the second passage close to L_3, and the orthogonal crossing at the fifth intersection with the x axis. They are, therefore, zeros of $x'_5(\mu)$. These zeros give rise to sequences $\{\mu_{l,m}^{1,\overline{3}-}\}_m$ and $\{\mu_{l,m}^{1,\overline{3}+}\}_m$.

Concerning the function $x'_4(\mu)$ (see Fig. 10, left), we remark a main difference with the function $x'_3(\mu)$. We have just seen that, related to μ values in Λ_2, there is a finite number of values of Λ_3, which all together accumulate to μ_l^1. Instead of this, magnifications of Fig. 10 show that, associated to each value in Λ_2, there is an infinity of values in Λ_4 accumulating to it, giving rise to a double infinity of values of Λ_4 accumulating to μ_l^1. This is due to the fact that SHO in Λ_4 are two–round with respect to SHO in Λ_2, so the theoretical results in Grotta Ragazzo (1997); Mielke et al. (1992) imply the existence of an infinity of SHO in Λ_4 for each SHO in Λ_2. Taking loops into account, we obtain sequences $\{\mu_{l,m,k}^{1,2\pm,4\pm}\}_{m,k}$, $\{\mu_{l,m,k}^{1,2\pm,\overline{4}\pm}\}_{m,k}$, $\{\mu_{l,m,k}^{1,\overline{2}\pm,4\pm}\}_{m,k}$, $\{\mu_{l,m,k}^{1,\overline{2}\pm,\overline{4}\pm}\}_{m,k}$.

With respect to the function $x'_5(\mu)$, Fig. 10 shows that its behavior relative to $x'_4(\mu)$ is very similar to the behavior of $x'_3(\mu)$ with respect to $x'_2(\mu)$. We therefore have sequences $\{\mu_{l,m}^{1,5\pm}\}_m$, $\{\mu_{l,m}^{1,\overline{5}\pm}\}_m$. The fact that the obtained graph for $x'_5(\mu)$ has some thickness instead of being an smooth curve reveals that we are approaching the limit of numerical accuracy.

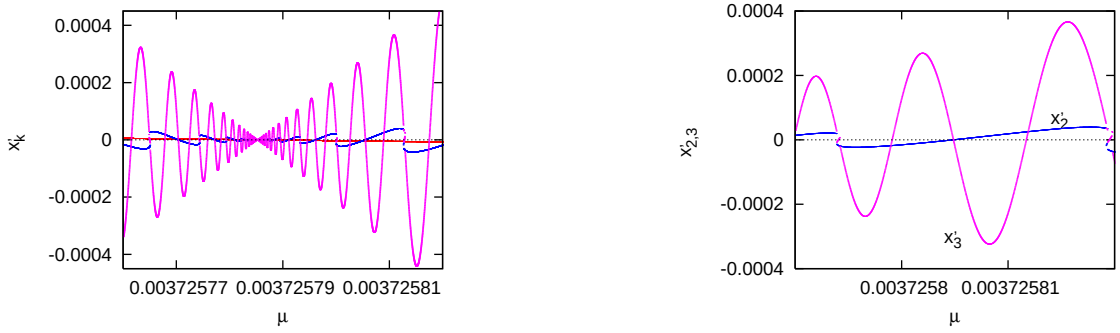

Figure 9: Left: functions $x'_k(\mu)$, for $k = 1$ (in red), $k = 2$ (in blue), $k = 3$ (in magenta). Right, the same functions for $k = 2, 3$ in a range corresponding to two consecutive discontinuities of $x'_2(\mu)$, where three zeros of $x'_3(\mu)$ exist (see the text for more details).

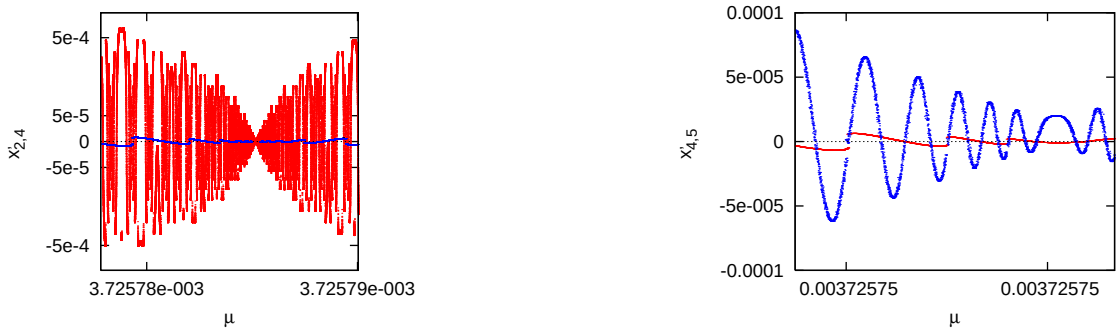

Figure 10: Letf: functions $x'_2(\mu)$ and $x'_4(\mu)$. For display purposes, the function x'_4 has been rescaled using the arcsinh(x) function, and the y axis has been labeled accordingly. Right: functions $x'_4(\mu)$, $x'_5(\mu)$.

7 Conclusions

In this paper, a numerical study of multi-round, horseshoe-shaped homoclinic connections of the L_3 point of the restricted three-body problem, varying the μ parameter, has been done. We have examined the existence of *simple* (one round) homoclinic connections to L_3. We have found that there exist two sequences of values of μ tending to zero for which a one round homoclinic connection exists. The difference between the two sequences is in the number of intersections of the orbit with the horizontal axis: in one case there is only one intersection, while in the other there are three due to the presence of a loop at $y = 0$. Next, for each fixed value of μ corresponding to a one-round homoclinic connection, the existence of multi-round homoclinic orbits has been studied. The analytical results in Grotta Ragazzo (1997); Mielke et al. (1992) show that there exists a cascade phenomenon of multi-round homoclinic orbits in the parameter value μ tending to that fixed value. We have illustrated this fact for two, three and four-round homoclinic connections to the L_3 point, pointing out the similarities and differences on the results obtained depending on the number of revolutions considered.

8 Acknowledgements

E. Barrabés and J.M. Mondelo are partially supported by the MCyT/FEDER grants BFM2003-09504-C02-01 and MTM2006-05849/Consolider. J.M. Mondelo is also supported by the MCyT/FEDER grant MTM2005-02139. M. Ollé is partially supported by the MCyT/FEDER grant MTM2006-00478.

References

Barrabés, E. and S. Mikkola (2005). Families of periodic horseshoe orbits in the restricted three-body problem. *Astronomy & Astrophysics 432*, 1115–1129.

Barrabés, E., J. M. Mondelo, and M. Ollé (2008). Numerical continuation of families of homoclinic connections of periodic orbits in the RTBP. *Preprint*.

Barrabés, E. and M. Ollé (2006). Invariant manifolds of L_3 and horseshoe motion in the restricted three-body problem. *Nonlinearity 19*, 2065–2089.

Bernard, P., C. Grotta Ragazzo, and P. A. Santoro Salomão (2003). Homoclinic orbits near saddle-center fixed points of Hamiltonian systems with two degrees of freedom. *Astérisque* (286), xviii–xix, 151–165. Geometric methods in dynamics. I.

Canalias, E. (2007). *Contribution to Libration Orbit Mission Design using Hyperbolic Invariant Manifolds*. Ph. D. thesis, Universitat Politécnica de Catalunya.

Canalias, E. and J. J. Masdemont (2006). Homoclinic and heteroclinic transfer trajectories between planar Lyapunov orbits in the sun-earth and earth-moon systems. *Discrete Contin. Dyn. Syst. 14*(2), 261–279.

Connors, M., P. Chodas, S. Mikkola, P. Wiegert, C. Veillet, and K. Innanen (2002). Discovery of an asteroid and quasi-satellite in an earth-like horseshoe orbit. *Meteoritics & Planetary Science 37*, 1435–1441.

Devaney, R. (1977). Blue sky catastrophes in reversible and Hamiltonian systems. *Ind. Univ. Math. 26*, 247–263.

Farrés, A. (2005). Stability regions around the Lagrangian points in the RTBP and their boundaries. Master's thesis, Universitat de Barcelona.

Font, J. (1999). *The role of homoclinic and heteroclinic orbits in two-degrees of freedom Hamiltonian systems*. Ph. D. thesis, University of Barcelona.

Gómez, G., A. Jorba, J. Masdemont, and C. Simó (2001). *Dynamics and Mission Design Near Libration Point Orbits – Volume 4: Advanced Methods for Triangular Points*. World Scientific. Reprint of ESA Report *Study of Poincaré Maps for Orbits Near Lagrangian Points*, 1993.

Gómez, G., W. S. Koon, M. W. Lo, J. E. Marsden, J. Masdemont, and S. D. Ross (2004). Connecting orbits and invariant manifolds in the spatial Restricted Three-Body Problem. *Nonlinearity 17*(5), 1571–1606.

Gómez, G., M. Marcote, and J. M. Mondelo (2005). The invariant manifold structure of the spatial Hill's problem. *Dynamical Systems. An International Journal 20*(1), 115–147.

Gómez, G. and J. J. Masdemont (2000). Some zero cost transfers between Libration Point orbits. *Advances in the Astronautical Sciences 105*, 1199–1216.

Gómez, G., J. J. Masdemont, and J. M. Mondelo (2003). Libration Point Orbits: A survey from tye dynamical point of view. In G. Gómez, M. W. Lo, and J. J. Masdemont (Eds.), *Libration Point Orbits and Applications*. World Scientific.

Grotta Ragazzo, C. (1997). Irregular dynamics and homoclinic orbits to Hamiltonian saddle centers. *Comm. Pure Appl. Math. 50*(2), 105–147.

Henrard, J. (1973). Proof of a conjecture of e. strömgren. *Celestial Mechanics and Dynamical Astronomy 7*, 449–457.

Henrard, J. and J. F. Navarro (2004). Families of periodic orbits emanating from homoclinic orbits in the restricted problem of three bodies. *Celestial Mechanics and Dynamical Astronomy 89*, 285–304.

Howell, K. C., B. T. Barden, R. S. Wilson, and M. W. Lo (1998). Trajectory design using a dynamical systems approach with application to GENESIS. *Advances in the Astronautical Sciences 97*, 1665–1684.

Koltsova, O., L. Lerman, A. Delshams, and P. Gutiérrez (2005). Homoclinic orbits to invariant tori near a homoclinic orbit to center-center-saddle equilibrium. *Phys. D 201*(3-4), 268–290.

Koltsova, O. Y. (2003). Families of multi-round homoclinic and periodic orbits near a saddle-center equilibrium. *Regul. Chaotic Dyn. 8*(2), 191–200.

Koltsova, O. Y. and L. M. Lerman (1995). Periodic and homoclinic orbits in a two-parameter unfolding of a hamiltonian system with a homoclinic orbit to a saddle-center. *Int. J. Bifurcation and Chaos 5*(2), 397–408.

Koon, W. S., M. W. Lo, J. E. Marsden, and S. D. Ross (2000). Heteroclinic connections between periodic orbits and resonance transitions in celestial mechanics. *Chaos 10*(2), 427–469.

Lerman, L. M. (1991). Hamiltonian systems with loops of a separatrix of a saddle-center [translation of *methods of the qualitative theory of differential equations* (Russian), 89–103, Gor′kov. Gos. Univ., Gorki, 1987]. *Selecta Math. Soviet. 10*(3), 297–306. Selected translations.

Llibre, J., R. Martínez, and C. Simó (1985). Transversality of the invariant manifolds associated to the Lyapunov family of periodic orbits near L_2 in the restricted three-body problem. *J. Differential Equations 58*(1), 104–156.

Llibre, J. and M. Ollé (2001). The motion of Saturn coorbital satellites in the restricted three-body problem. *Astronomy and Astrophysics 378*(3), 1087–1099.

Mcgehee, R. P. (1969). *Some homoclinic orbits for the restricted three-body problem.* Ph. D. thesis, University of Wisconsin.

Mielke, A., P. Holmes, and O. O'Reilly (1992). Cascades of homoclinic orbits to, and chaos near, a Hamiltonian saddle-center. *J. Dynam. Differential Equations 4*(1), 95–126.

Parker, J. S. and M. W. Lo (2006). Shoot the moon 3D. *Advances in the Astronautical Sciences 123*, 2067–2086.

Schanzle, A. J. (1967). Horseshoe-shaped orbits in the jupiter-sun restricted problem. *The Astronomical Journal 72*(2), 149–157.

Simó, C. (2006). Boundaries of stability. talk given at Univ. de Barcelona, Jun 3. Available at `maia.ub.edu/dsg/`.

Szebehely, V. (1967). *Theory of Orbits. The Restricted Problem of Three Bodies.* Academic Press, Inc.

Taylor, D. B. (1981). Horseshoe periodic orbits in the restricted problem of three bodies for a Sun-Jupiter mass ratio. *Astronom. and Astrophys. 103*(2), 288–294.

Wilczak, D. and P. Zgliczyński (2003). Heteroclinic connections between periodic orbits in planar restricted circular three-body problem—a computer assisted proof. *Comm. Math. Phys. 234*(1), 37–75.

Wilczak, D. and P. Zgliczyński (2005). Heteroclinic connections between periodic orbits in planar restricted circular three body problem. II. *Comm. Math. Phys. 259*(3), 561–576.